Efficiency and Damping Control Evaluation of a Matrix Converter with a Boost-up AC Chopper in Adjustable Speed Drive System

Kazuhiro Koiwa and Jun-ichi Itoh
Department of Electrical Engineering
Nagaoka University of Technology
1603-1 Kamitomioka-machi Nagaoka, Japan
itoh@vos.nagaokaut.ac.jp

Abstract— **This paper evaluates the damping control for a matrix converter (MC) configuration with a boost-up AC chopper and the efficiency characteristics. This circuit configuration can improve the voltage transfer ratio, but the losses are increased due to the additional AC chopper. On the other hand, as a motor is driven at high rotating speed region, the flux-weakening control is necessary for general MCs. However, the copper loss is increased due to the flux-weakening control when an IPMSM is used. Therefore, the validity of the proposed circuit is evaluated in IPMSM adjustable speed drive system in term of efficiency. In addition, the proposed circuit is demonstrated by 3.7-kW prototype in simulation and experiments. As a result, it is revealed that the efficiency of the proposed system is higher when the motor rated voltage is over 107% of the input voltage.**

I. INTRODUCTION

The matrix converters (MCs) which can convert an AC power supply voltage directly into an AC output voltage of variable amplitude and frequency without the large energy storages, such as electrolytic capacitors, have been studied recently [1-3]. However, one of the disadvantages of the MC is that the voltage transfer ratio, which defines as the ratio between the output voltage and the input voltage, is being constrained to 0.866. In terms of the motor drive system, even a PM motor can be driven at rated frequency by an MC after applying the flux-weakening, however, the output current is increased and as a result the efficiency is reduced [3-4]. Therefore, in considering of widely applying the MC in the near future, the boost-up functionality is important.

In order to solve this problem, a Matrix-Reactance Frequency Converter (MRFC), which consists of a MC and an AC chopper, has been studied [5]. Reference [5] shows that the amplitude of the output voltage is controlled the voltage which is higher than the input voltage. However the MRFC requires many components including the boost-up reactor and capacitor. In addition, the control of the MRFC becomes complicated because the regular synchronizing between the MC and the chopper is required.

The authors previously proposed a circuit topology which connects a V-connection AC chopper at the input stage of the MC that enables boost-up functionality in order to overcome the problem of voltage transfer ratio [6-8]. As a result, it is not necessary to add the large inductor at primary stage of the AC chopper. Therefore, the V-connection AC chopper and these components do not dominate the size and the weight in comparison to the origin structure of a MC. However, the proposed circuit has some problems as follows: (i) the resonance occurs in the input filter, and (ii) additional losses caused by the AC chopper. Thus, it is important to suppress the input filter resonance and to evaluate the total losses in comparison with that of the conventional MC.

In this paper, in order to suppress the input filter resonance, the damping control is applied in either the AC chopper or the MC. Three different types of the damping controls are studied to apply in the proposed system, that is, (i) the current-type, (ii) the voltage-type and (iii) the output-side damping control. However, the characteristic of each damping controls has not been discussed and compared in the adjustable speed drive system. On the other hand, the validity of the proposed system is evaluated in the adjustable speed drive system in order to clarify the advantage of the proposed system. Concretely, in order to drive the motor at high speed, there are two possible solutions: (i) to apply the flux-weakening control or (ii) to boost-up the voltage by the AC chopper. However, the method that can ensure high efficiency is not clear since the output voltage is limited. Thus, in order to confirm the effectiveness of the proposed system, it is important to evaluate the total losses in comparison with the conventional MC when the boost-up ratio is subjected to changes.

The constitutions of the paper are follows: first, the three damping control methods are explained. Next, the losses in the proposed circuit and the conventional MC are discussed theoretically. Finally, the operation of the proposed system will be demonstrated experimentally in a 3.7-kW Interior Permanent Magnet Synchronous Motor (IPMSM). In

addition, the chopper and the copper losses are evaluated to clarify the validity of the proposed system.

II. Circuit Toporogy and Damping Control Strategy

Fig. 1 shows the proposed circuit which connects a V-connection AC chopper at the input stage of the MC. The relationship between the input voltage v_{in} and the output voltage v_{out} is expressed by

$$v_{out} = \beta \cdot \lambda_{mc} \cdot v_{in} \quad (1),$$

where, λ_{mc} is the modulation index of the MC, β is the boost-up ratio of the chopper and v_{in} is the input voltage. Basically, the function of the AC chopper is simply boost-up the input voltage. A feedback control is not required for the filter capacitor since both the input and output sides of the AC chopper are AC voltage. Therefore, the capacitor value is not dominated by the voltage control response and the current response of the input side in compared with a Back-to-Back (BTB) system which consists of a PWM rectifier and an inverter. As a result, the V-connection AC chopper and its components are not dominated by the volume and the weight in comparison to the origin structure of a MC. However, the resonance between the input filter of the MC and the AC chopper occurs in the proposed circuit. Therefore, the damping control is needed to suppress the resonance.

Fig. 2 shows the control diagram of the three type damping control methods for the proposed circuit. Several studies have discussed and illustrated the features of each of the damping controls [8-10]. Due to the differential in characteristic, a suitable damping control is therefore selected according to the application. Fig. 2(a) shows the block diagram of the current-type damping control [8]. The input currents are detected and treated as signals for the damping control. Additionally, the high pass filter (HPF) is used to decouple the oscillation components that are produced from the input current. In the current-type, even the resonance distortion can be suppressed, current sensors are necessary to implement physically due to the requirement of current feedback. In contrast, Fig. 2(b) shows the control diagram of the voltage-type damping control, where the current sensors are not required [9]. The operation of the voltage-type is follows: first, the capacitor current i_c is estimated from the differentiation of the capacitor voltage v_c. However, due to the noise disturbance, an HPF is used as a pseudo differentiation. The cost of the voltage-type damping control is cheaper than the current-type because the additional sensors are not needed. Finally, Fig. 2(c) shows the control diagram of the output damping control which is applied in the MC [10]. The harmonic distortion in the input stage can be suppressed by suppressing the harmonic distortion in the output stage. This is because the input instantaneous power is equaled to the output instantaneous power in the MC.

As a result, the features of the damping control can be summarized as follows:(i) The current-type can achieve low harmonic components in the input current THD, (ii) the voltage-type can effectively suppress the resonance without additional sensors, which is benefits in terms of cost, and (iii) the output damping control can simplify the overall control system. The effectiveness of the damping controls in terms of experimental will be continue to discuss in the chapter IV.

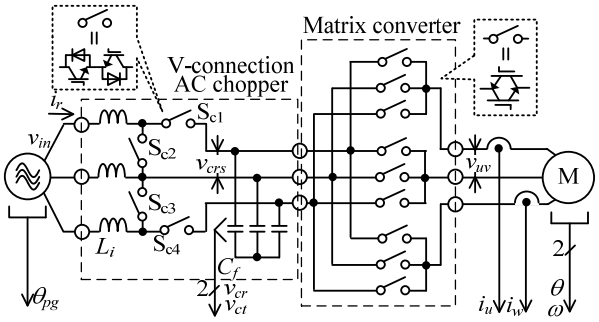

Figure 1. Circuit configuration of matrix converter with boost-up chopper. In order to compensate output voltage, V-connection AC chopper is connected at input side.

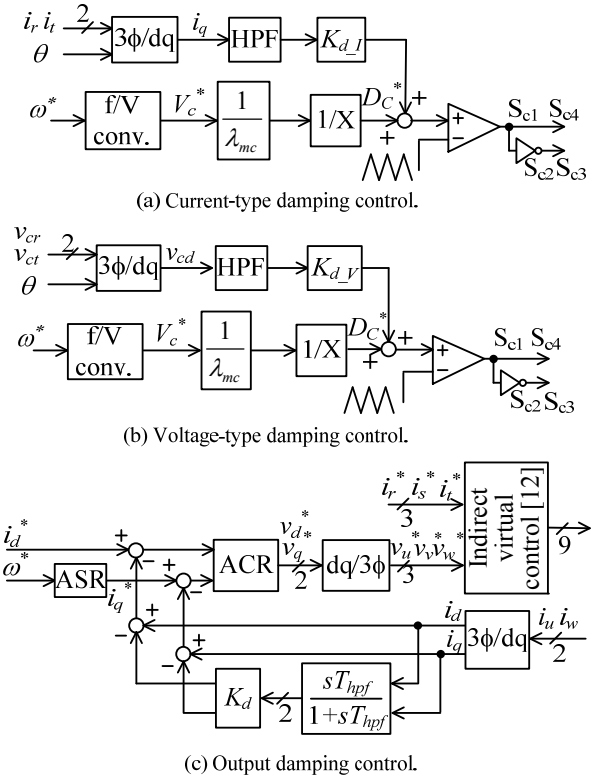

Figure 2. Control diagram of the damping controls. Current-type can achieve low THD. Voltage-type can suppress the resonance without additional sensors. Output-side can simplify the overall control system.

III. Derivation Method of Chopper Loss and Copper Loss

A. Chopper loss

In order to consider the influence of the chopper loss for the proposed system, the chopper losses such as the

conduction loss and the switching loss are theoretically derived in this section.

First, the conduction loss of S_{c1} is expressed by

$$P_{conS1} = \frac{1}{\pi}\int_0^{\pi} v_{ce} i_r d\omega t \tag{2}$$

where, v_{ce} is the on-state voltage of S_{c1} which is expressed by (3) and i_r is the input current.

$$v_{ce} = k_{con1} i_r + k_{con2} \tag{3}$$

Note that k_{con1} and k_{con2} are coefficient as defined from the on-state voltage characteristics in the datasheet of the switching device. In this paper, SK80GM063 from SEMIKRON is used as the switching devices in the AC chopper. The rated voltage and the rated current of this IGBT are 600V and 81A, respectively. From these equations, the conduction loss of S_{c1} is expressed by

$$P_{con\_S1} = \frac{k_{con1}}{\beta} I_{in}^{\ 2} + \frac{2\sqrt{2}}{\pi}\frac{k_{con2}}{\beta} I_{in} \tag{4}$$

where, I_{in} is the effective value of the input current. In similar, the conduction loss of S_{c2} is expressed by (5).

$$P_{con\_S2} = \frac{(\beta-1)k_{con1}}{\beta} I_{in}^{\ 2} + \frac{2\sqrt{2}}{\pi}\frac{(\beta-1)k_{con2}}{\beta} I_{in} \tag{5}$$

Note that the equations of the conduction loss of S_{c4} and S_{c3} are equal to (4) and (5), respectively.

Fig. 3 shows the integral period to calculate the switching loss. The switching loss of the AC chopper is proportional to the multiplication of the capacitor voltage v_{crs} and the input current i_r. Moreover, the integral period is different among each of the switching devices. In other words, the integral period for the S_{c1} and S_{c4} is to π from 5π/6, and the integral period for the S_{c2} and S_{c3} is to π from π/6. Thus, the switching loss P_{ton_s1} and P_{ton_s2} are expressed by

$$\begin{aligned} P_{ton\_S1} &= \frac{1}{\pi}\int_{\frac{5}{6}\pi}^{\pi} e_{on} f_s \frac{v_{rs}}{V_s} d\omega t \\ &= \frac{\sqrt{2}V_{in} f_s}{24\pi V_s}(\beta-1)[(\sqrt{6}\pi-6)k_{ton1} I_{in} + 12(\sqrt{3}-2)k_{ton2}] \end{aligned} \tag{6}$$

$$\begin{aligned} P_{ton\_S2} &= \frac{1}{\pi}\int_{\frac{\pi}{6}}^{\pi} e_{on} f_s \frac{v_{rs}}{V_s} d\omega t \\ &= \frac{\sqrt{2}\beta V_{in} f_s}{24\pi V_s}[(5\sqrt{6}\pi + 3\sqrt{2})k_{ton1} I_{in} + 12(1+\sqrt{3})k_{ton2}] \end{aligned} \tag{7}$$

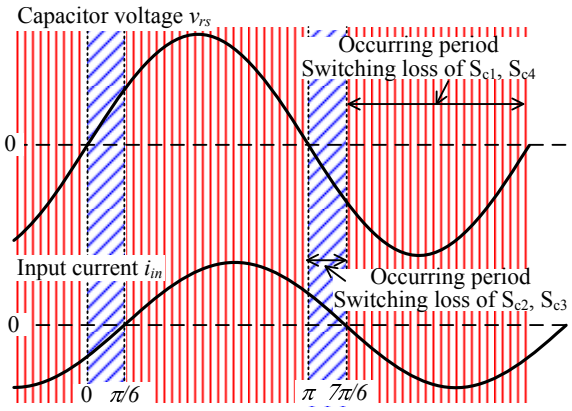

Figure 3. Integral period of switching loss of AC chopper. Switching loss occurs during different period among each switching devices.

TABLE I. CALCULATION PARAMETERS TO CALCULATE CHOPPER LOSS. PARAMETERS OF SWITCHING DEVICE ARE OBTAINED FROM DATASHEET.

Parameters of switching device(SK80GM063)			Configuration system	AC chopper
On-state voltage characteristic	k_{con1} (V/A)	0.0182	Stray inductance	–
	k_{con2} (V)	0.9773	Stray capacitance	
Switching loss characteristic	k_{ton1} (J/A)	0.00005	Load	Constant current source
	k_{ton2} (J)	0.0		
Boost-up ratio of AC chopper β		1.15	Input reactor L_i	2 mH
Input line voltage V_{in}		200 V	Filter capacitor C_f	14.2 μF
Switching frequency f_s		10 kHz	Damping resistor R_d (connected at C_f)	1.0 Ω
Nominal voltage at switching test V_s		300 V		

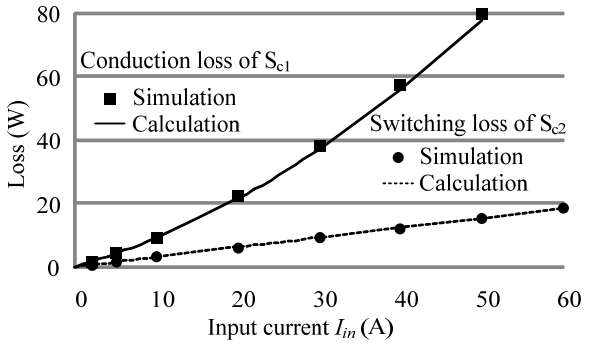

Figure 4. Chopper loss which are conduction loss and switching loss, for input current by calculation and simulation results.

where, V_s is the nominal voltage when the switching loss characteristics in the datasheet is used and f_s is the switching frequency of the AC chopper. In addition, e_{on} is the instantaneous switching loss which is characterized by (8).

$$e_{on} = k_{ton1} i_{in} + k_{ton2} \tag{8}$$

Note that k_{ton1} and k_{ton2} are the coefficients defined from the switching loss characteristics in the datasheet of the switching device. Furthermore, the equations of the switching loss of S_{c4} and S_{c3} are equal to (6) and (7).

In order to validate these equations, the calculation results are compared with the simulation results which are obtained from PSIM simulator. Table 1 shows the calculation parameters. In the simulation, only the AC chopper is simulated and current source is used as the load, in addition, the stray inductance and the stray capacitance are not taken into the consideration.

Fig. 4 shows the conduction and switching losses of the AC chopper by the theoretical calculation and the simulation [11]. Note that the chopper loss of the calculation results is the sum of the equations of (4), (5), (6) and (7). As a result, the calculation results are well agreed with the simulation results. Thus, the validity of the derived equations of the chopper loss is confirmed. In other words, the chopper loss can be easily calculated from the input current.

B. Copper loss by flux-weakening control

As an IPM motor is driven at high rotating speed region, it is necessary to apply the flux-weakening control in the motor control. However, the copper loss of the IPM motor is increased because the d-axis current is flowed by the flux-weakening control. In this section, the control strategy of the proposed system such as the flux-weakening control is explained. Additionally, the equation of the copper loss which is increased by the flux-weakening control, is introduced from the d-axis and q-axis current. In order to drive an IPM motor in high rotating speed area within the output voltage limitation of the MC, the flux-weakening control is necessary to apply in the MC control. This is because the back electromotive force becomes higher with increasing the rotating speed. The output voltage which is necessary to control the motor can be degraded by the flux-weakening control. Therefore, the d-axis current i_d for the flux-weakening control is introduced.

Fig. 5 shows a vector diagram in the flux-weakening control, where e_q is the back electromotive force, v and v' are the terminal voltage in the IPM motor without/with the flux-weakening control, respectively. Note that the winding resistance of the IPM motor R_w is not considered. The flux-weakening control in the IPM motor can equally weaken the magnetic flux in the permanent magnet from the d axis armature magnetic flux. As a result, the rotation speed area can be extended by implementing the flux-weakening control. From Fig. 5, V_{om} which is the maximum the output phase voltage of the MC, is expressed by (9).

$$V_{om} = \sqrt{{v_d}^2 + {v_q}^2} = \sqrt{(\omega L_q i_q)^2 + (\omega L_d i_d + e_q)^2} \tag{9}$$

Therefore, the d-axis current in the flux-weakening control at the maximum voltage is calculated by (10).

$$i_d = \frac{-e_q + \sqrt{{V_{om}}^2 - (\omega L_q i_q)^2}}{\omega L_d} \tag{10}$$

The motor current is increased after implementing due to the flux-weakening control, therefore the motor loss and the converter loss are increased. In order to validate the AC chopper, it is evinced that the copper loss is lower in the proposed system. In particular, previous equation has shown that the copper loss is subjected to the input line voltage.

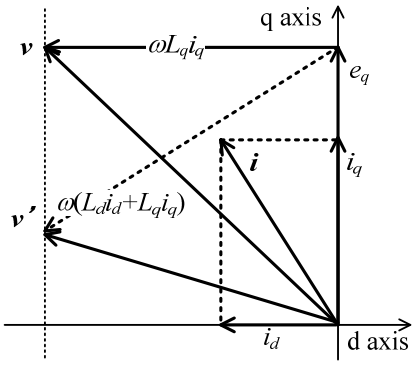

Figure 5. Vector diagram on flux-weakening control. In order to suppress output voltage, d-axis current is flowed negatively. Motor can be driven at high rotating speed by flux-weakening control.

TABLE II. IPM MOTOR PARAMETERS. COPPER LOSS IS CALCULATED FROM THESE PARAMETERS.

Rated mechanical power P_m	3.7 kW	Winding resistance R_w	0.693 Ω
Back electro-motive force e_q	151 V	d-axis inductance L_d	6.2 mH
Rated voltage V_n	180 V	q-axis inductance L_q	15.3 mH
Rated current I_n	14 A	Inertia moment J	0.0212 kgm^2
Synchronous speed ω_s	1800 rpm	Number of pole pairs P_n	3
Rated torque T_{eR}	19.6 Nm		

First, the torque of an IPM motor is expressed by (11).

$$T = P_n[\frac{e_q}{\omega} i_q + (L_d - L_q) i_d i_q] \tag{11}$$

where, P_n is the number of pole pairs. From (11), the torque of the IPM motor depends on the d-axis current and the q-axis current. From (10) and (11), the d-axis current and q-axis current depend on V_{om}. Additionally, V_{om} is decided by the input line voltage and voltage transfer ratio. In other words, in order to calculate the copper loss of the motor as V_{in} is changed, the q-axis current is introduced for V_{om}. Thus, V_{om} is expressed by (12) from (10) and (11).

$$V_{om} = \sqrt{[\frac{L_d}{(L_d - L_q)}(\frac{\omega T}{P_n} - \frac{L_q}{L_d} e_q i_q)\frac{1}{i_q}]^2 + (\omega L_q i_q)^2} \tag{12}$$

Note that the q-axis current should be obtained in order to derive the copper loss. However, Eq. (12) cannot obtain the q-axis current. For this reason, the q-axis current is calculated by numerical analysis. It should be noted that the q-axis current is limited by (13).

$$\left|i_q\right| \le \frac{V_{om}}{\omega L_q} \tag{13}$$

On the other hand, the d-axis current can be calculated by (10). Therefore, the copper loss P_c is expressed by (14).

$$P_c = 3R_w I_o^{\,2} = 3 \cdot R_w \cdot \frac{(i_d^{\,2} + i_q^{\,2})}{2} \tag{14}$$

where, R_w is the primary winding resistance of the IPM motor. Moreover, I_o is the R.M.S. value of the output current.

C. Comparison with chopper loss to copper loss

Fig. 6 shows the calculation results which comparing between the additional loss due to the AC chopper and the flux-weakening control. Note that the copper loss was calculated from the motor parameter which is shown in Table 2. Furthermore, additional copper loss in Fig. 6 subtracts copper loss due to the flux-weakening control P_{C_CMC} from that of the proposed system P_{C_BMC}. The copper loss of the proposed system does not depend on the input voltage because the output voltage is constantly control at 180V by the AC chopper. On the other hand, when the input voltage is degraded, the output voltage of the conventional MC is decreased due to limited voltage transfer ratio. In addition, the flux-weakening control in the IPM motor is not capable of wide range application. Therefore, in order to extend the applications, the input voltage of the proposed system and the conventional MC are degraded. Then, high rotating speed of the IPM motor is possible to be simulated. From the result, there is a range that additional copper loss(P_{C_CMC} - P_{C_BMC}) is negative. This is because the copper loss in the proposed system is larger than that of conventional MC. Additionally, in case that the ratio between the motor rated voltage V_n and input voltage V_{in} (V_n/V_{in}) is less than 1.01 p.u., the chopper loss is larger than the copper loss. On the other hand, as V_n/V_{in} gets higher than 1.01 p.u., the chopper loss is lower than the copper loss. This is because the motor current and the copper loss are increased due to the flux-weakening control when V_n/V_{in} is higher.

Therefore, as the motor parameters and the switching device characteristics are known, the effective region of the AC chopper can be calculated by (4), (5), (6), (7), (10) and (12). In other words, it is not necessary to analyze the total loss by the experiment. In terms of efficiency, effectiveness of the proposed system can be evaluated from the conventional MC by using the motor parameter and the device parameter without experiment.

IV. Experimental Results

A. Acceleration results of IPMSM

Fig. 7 shows the experimental acceleration tests for the IPM motor which is driven by the proposed system with vector control. Note that 4-step commutation sequence, which uses the filter capacitor voltage, is applied to the

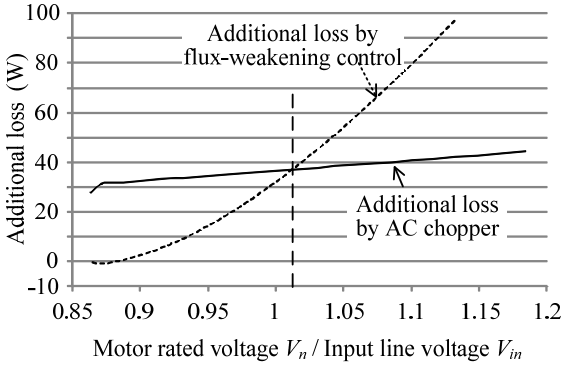

Figure 6. Loss comparison between chopper loss and copper loss of motor by calculation when input line voltage is changed. Copper loss in the figure subtracts copper loss which occurs by the conventional MC PC_CMC from the copper loss by the proposed system PC_BMC.

TABLE III. Experimental Conditions.

Rotating speed ω		1800 rpm	Output control	Vector control
Input frequency		50 Hz	Commutation	Voltage-type
Carrier frequency	Chopper	10 kHz	MC control	Virtual indirect control
	MC			
Response angular frequency ω_r	ACR	3000 rad/s	Load	3.7-kW IPM motor
	ASR	200 rad/s		
Input reactor L_i		2 mH	Switch of MC	18MBI100W-120A
Filter capacitor C_f		14.2 μF	Switch of chopper	SK80GM063
Damping resistor R_d (Conventional MC)		32.7 Ω		

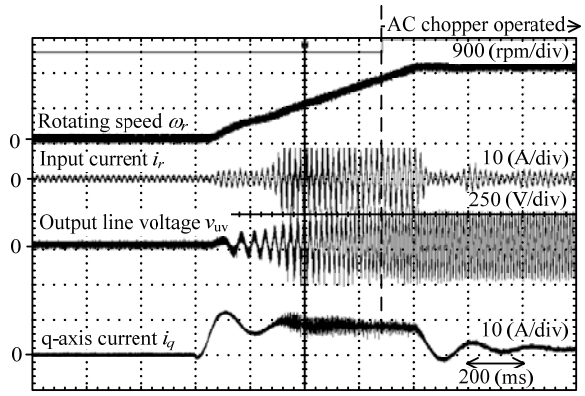

Figure 7. Experimental acceleration test by MC with boost-up chopper. Acceleration time is 0.8s. Boost-up AC chopper operates during rotating speed is over 1560 r/min.

experiment. In Fig. 7, the AC chopper starts operating while the rotating speed command ω^* is over 1560rpm, and then the damping control is applied to suppress the input filter resonance. Additionally, it is confirmed that the input and q-axis current are not drastically changed as the AC chopper is started operating. Therefore, the proposed system can continuously improve the voltage transfer ratio of the MC.

Fig. 8 shows the output line voltage characteristic based on the output power of the converter. In this paper, the flux-weakening control is applied within rated voltage of the motor when the load torque is changed at rated speed. Note

that the input line voltage is set to 180V. According to the result, it is confirmed that the output line voltage is limited up to 180V by the flux-weakening control. Thus, the flux-weakening control is validated by the experimental results. When the load torque is changed at rated speed of the motor, the flux-weakening control is applied at 1.3-kW output power of the converter by the proposed system. On the other hand, the flux-weakening control is started to apply at 400-W output power of the converter. In other words, as the output power of the converter is over 400-W load, the d-axis current become larger due to the flux-weakening control by the conventional MC. As a result, the copper loss is increased due to the flux-weakening control.

B. Evaluation of damping controls

Fig. 9(a) shows the torque transient operation without the damping control. Note that the motor cannot be rotated due to the harmonic distortion that is occurred in the case of without the damping control when the load torque is changed from 0% to 100%. Therefore, the torque step is degraded to 60% so that the motor can be rotated even the damping control is not applied. As a result, the convergence time of the rotating speed ω is approximately 41.4ms. On the other hand, Fig. 9(b) shows the torque transient operation with the output-side damping control. As a result, the convergence time of ω is approximately 46.2ms. Additionally, the overshoots of the i_d and i_q are larger than that of the case of Fig. 9(a). The cause of the overshoot is to apply the output damping control which compensates the transient component of the i_d and i_q. Next, Fig. 9(c) shows the torque transient operation with the current-type damping control. From the results, the convergence time of ω is approximately 41.4ms, which is similarly to Fig. 9(a). Finally, Fig. 9(d) shows the torque transient operation with the voltage-type damping control. Similarly, the convergence time of ω is approximately 42.8ms.

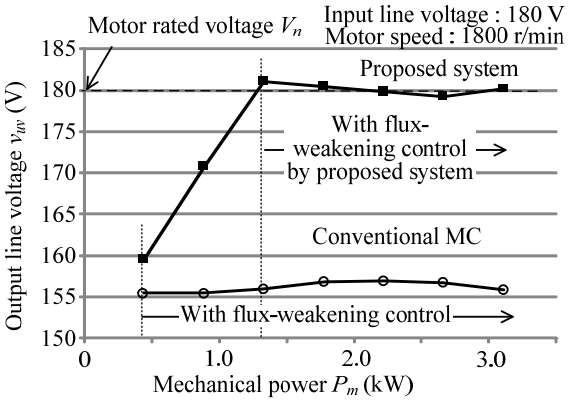

Figure 8. Output line voltage characteristic with flux-weakening control. Note that the input line voltage is set to 180V. As a result, the output line voltage is limited up to 180V by the flux-weakening control.

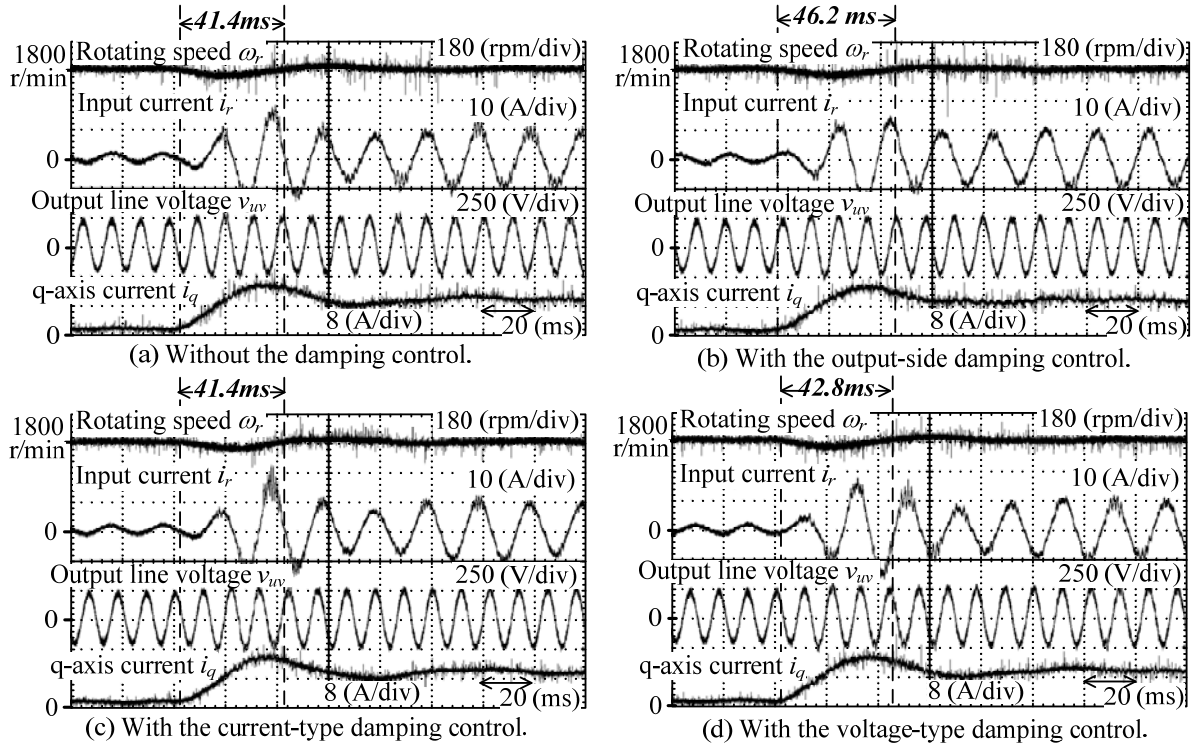

Figure 9. Transient waveforms by each damping controls. As simulation time is 0.1s, load torque changes from 0% to 60%. The convergence time of ω are follows: (a) 41.4 ms, (b) 46.2 ms, (c) 41.4 ms and (d) 42.8 ms. The current-type is better than the other damping controls because the convergence time of ω is not changed by applying the damping control.

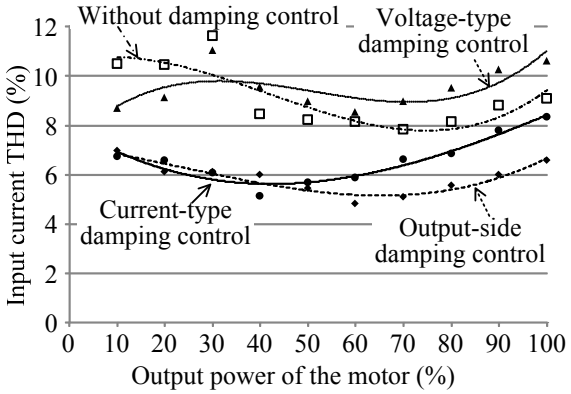

Figure 10. Input current THD characteristics by without and with the damping control. The input current THD is lower than 7% by the output-side damping control.

Fig. 10 shows THD (Total Harmonic Distortion) of the input current among the applied damping controls. From the result, the input current THD can achieve lower than 7% at almost all power ranges with the implementation of the output-side damping control. Accordingly, the damping effect of the output-side is higher than that of others damping controls.

C. Loss analysis of conventional MC and proposed system

In order to validate the proposed system in terms of the efficiency, the total loss characteristic of the proposed system is compared to the conventional MC by the simulations and the experiments.

Fig. 11 shows the converter efficiency characteristic and the input power factor characteristic, proportional to the output power of the MC. First, it is confirmed that the unity power factor can be obtained in more than 1-kW output power. On the other hand, the converter efficiency at maximum point is 94.8% at 2.3-kW output power.

Fig. 12 shows the d-axis current and the q-axis current characteristics. Note that the experimental result was obtained by the proposed system. In order to validate the equation of the copper loss, the calculation results are compared to the experimental results. According to Fig. 12-(a), the calculation result is almost agreed with the experimental result. On the other hand, in Fig. 12-(b), the error between the calculation result and the experiment result is approximately 10%. This error is because the winding resistance of the IPM motor is not considered in (13). However, the trend of the calculation result almost agrees with the experimental result. Thus, the validity of the equations for the copper loss can be confirmed. Besides, as the ratio of V_n/V_{in} gets larger, the d-axis current becoming larger. It means that the compensation value of the flux-weakening control is increased with the ratio of V_n/V_{in}. On the other hand, the q-axis current is decreased as the ratio of V_n/V_{in} is increased. According to (11), in case that the torque is constant, the q-axis current is decreased when the d-axis current is increased.

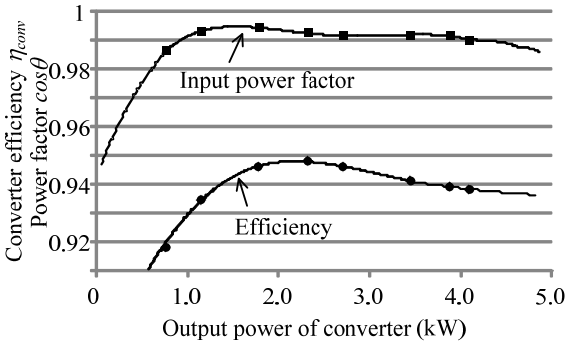

Figure 11. Converter efficiency and input power factor characteristics of the proposed system. Converter efficiency at maximum point is 94.8% at 2.3-kW output power.

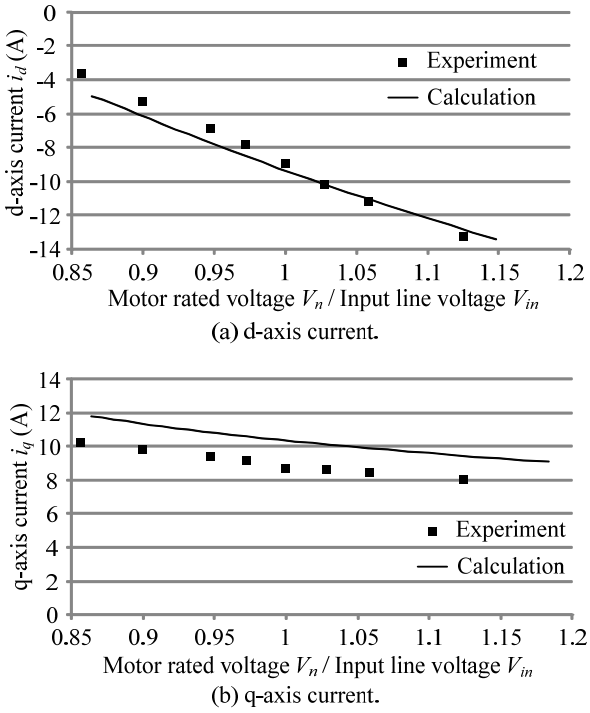

Figure 12. d-axis current and q-axis current comparison between calculation and experimental results by the proposed system. Error between calculation and experimental result is within 10%.

Fig. 13 shows the total loss comparison between the proposed system and the conventional MC. Note that the input voltage V_{in} was changed. Additionally, the iron loss and the mechanical loss P_{other} were obtained from the experiment by (16).

$$P_{other} = -125 \cdot (V_n / V_{in}) + 308 \quad (16)$$

Accordingly, the total efficiency of the conventional MC which is applying the flux-weakening control becomes low as the input line voltage is decreased. This is because the conduction loss of the converter and the copper loss of the IPM motor are becoming larger due to the flux-weakening

control. On the other hand, the AC chopper in the proposed system can easily improve the input line voltage which has been decreased. For this reason, high efficiency of the proposed system can be achieved in the adjustable drive system.

According to the experimental result, when the ratio of the input line voltage and motor rated voltage is over 1.07 p.u. , the total loss of the proposed system is less than that of the conventional MC. However, in comparison with Fig. 6, the turning point is different. The error between the calculation and experimental result is approximately 5.6%. The reason of this error is because the iron loss and mechanical loss is not considered in Fig. 6. The iron loss is depending on the output line voltage and frequency. Therefore, the validity of the proposed system is revealed as the motor rated voltage is over 107% of the input voltage.

Fig. 14 shows the relationship between turning point of V_n/V_{in} and the output power of the converter. As the result, the turning point of V_n/V_{in} which becomes effectiveness of the proposed system, is degraded when the output power of the converter is increased. This is because the total efficiency of the conventional MC is drastically degraded in comparison with the proposed system when the output power of the converter increased. Thus, if the output power of the converter are increased, effectiveness of the proposed system can be expanded. In particular, it is revealed that the efficiency of the proposed system is higher than that of the conventional MC at the rated output power of the converter when the motor rated voltage is over 90% of the input voltage.

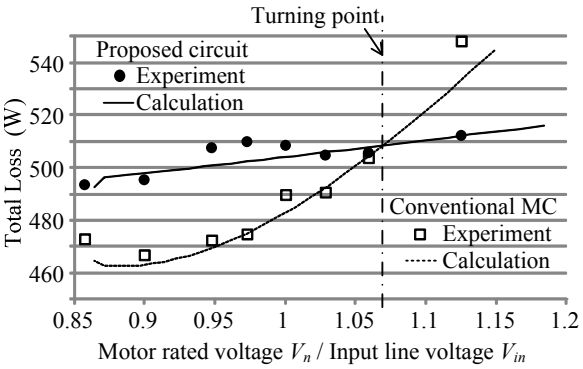

Figure 13. Total loss comparison between conventional MC and proposed system. In case that V_n/V_{in} is over 107%, total loss of the proposed system is less than the conventional MC.

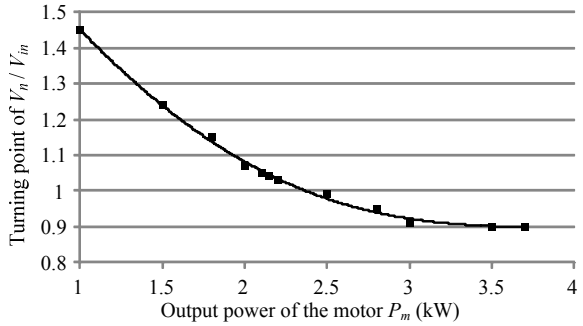

Figure 14. Relationship between the turning point of V_n/V_{in} and the output power of the motor P_m by calculation result. The turning point of V_n/V_{in} is the point that the total loss of the proposed system is lower than that of the conventional MC.

V. CONCLUSION

In this paper, the validity of the proposed circuit is evaluated in term of the efficiency in an IPMSM drive system. The proposed circuit was demonstrated by a 3.7-kW IPMSM. As a result, it can be accomplished that the validity of the proposed system is confirmed as the motor rated voltage is under 107% of the input voltage.

ACKNOWLEDGMENT

A part of this study was supported by Industrial Technology Grant Program in 2009 from New Energy and Industrial Technology Development Organization (NEDO) of Japan.

REFERENCES

[1] P. W. Wheeler, J. Rodriguez, J. C. Clare, L. Empringham: ”Matrix Converters: A Technology Review” IEEE Transactions on Industry Electronics Vol. 49, No. 2, pp274-288, 2002.

[2] Q. Lei, F.Z.Peng, B. Ge: "Pulse-Width-Amplitude-Modulated Voltage-Fed Quasi-Z-Source Direct Matrix Converter with maximum constant boost", , Vol. , No. , pp. 641-646 (2012)

[3] D. Casadei, M. Mengoni, G. Serra, A. Tani, L. Zarri: "Assessment of an Induction Motor Drive for High Speed Operation based on Matrix Converter", EPE2007, Vol. , No. , pp. (2007)

[4] Ki-Chan Kim : "A Novel Magnetic Flux Weakening Method of Permanent Magnet Synchronous Motor for Electric Vehicles", IEEE Trans., Vol. 48, No. 11, pp. 4042 - 4045 (2012)

[5] Shinn-Ming, Sue, Ching-Tsai Pan: “Voltage-Constraint-Tracking-Based Field-Weakening Control of IPM Synchronous Motor Drives", IEEE Transactions on Industrial Electronics, vol. 55, no. 1, pp. 340-347, 2008

[6] J. Itoh, H. Tajima, H. Ohsawa: “Induction Motor Drive System using V-connection AC Chopper”, IEEJ Trans., Vol.123, No.3, pp.271-277 (2003)

[7] T.Shinyama, M. Kawai, A. Torii, A. Ueda: “Characteristic of an AC Chopper Circuit with LC Filters in the Input and Output Side”, IEEJ Trans., Vol.125-D, No.3, pp.205-211 (2005)

[8] K. Koiwa, J. Itoh: "Experimental Verification of Effectiveness of Boost-up Matrix Converter with V-connection AC Chopper", IEEJ Trans. D, Vol. 132, No. 1, pp. 1-8 (2012)

[9] K. Koiwa, J. Itoh: "A damping control method for a matrix converter with a boost-up AC chopper ", Power Electronics and Motion Control Conference (IPEMC), 2012 7th International , Vol. 2, No. , pp. 783-789 (2012)

[10] H. Takahashi, J. Itoh: "Damping Control Method Combined to the Output Stage of a matrix Converter", , Vol. , No. 4, pp. 22-23 (2012)

[11] J. Itoh, T. Iida, A. Odaka:" Realization of High Efficiency AC link Converter System based on AC/AC Direct Conversion Techniques with RB-IGBT" Industrial Electronics Conference, Paris, PF-012149,2006

[12] J. Itoh, I. Sato, H. Ohguchi, K. Sato, A. Odaka and N. Eguchi: “A Control Method for the Matrix Converter Based on Virtual AC/DC/AC Conversion Using Carrier Comparison Method”, IEEJ Trans., Vol.124-D, No.5, pp.457-463 (2004)